Preparation and polymeric encapsulation of powder mineral pellets for self-healing cement based materials

R. Alghamri*, A. Kanellopoulos, C. Litina, A. Al-Tabbaa

*Department of Engineering, University of Cambridge CB2 1PZ, Cambridge, UK – e-mail: rami.j.alghamri@gmail.com

Abstract

Using mineral additives and admixtures as self-healing agents in cement-based composites has been extensively researched. However, if the minerals are added directly to the cementitious matrix without any protection, they could immediately react, leading to a decrease in self-healing efficiency with further associated side-effects on the mechanical properties of cementitious composites. Thus, this paper describes the development of coated pellets as a self-healing system in cement based materials. Pan pelletisation was utilised for producing pellets from three different powder minerals as potential healing agents: reactive magnesium oxide (MgO), silica fume and bentonite. Of these materials, two types of developed prototype pellets in addition to another two commercial types of MgO pellets with different pellet sizes were then encapsulated in a polyvinyl alcohol (PVA) based film coating. The PVA coating was evaluated for the apparent solubility in water and in alkaline solution, swelling property, water permeability, dynamic mechanical properties, and shell thickness on pellets. Although PVA coating exhibited a decrease in its mechanical properties in water or in the simulated concrete environment, it retained integrity and stability in both environments. The PVA shell thickness varied from 10 to 50 µm. As the coated pellets partially replaced the natural sand in mortar mixtures, they were characterised in comparison with sand for the particle size distribution, density, porosity, crushing strength and particle shape. Experimental results indicated that the different types of pellets showed higher porosity and lower crushing strength compared to sand. In mortar mixtures, the pellets showed excellent compatibility with minimal influence on the fresh mixture properties and the compressive strength of the hardened specimens. This was accompanied by good distribution inside the concrete matrix. Further investigations on the self-healing performance of these pellets are under way.

Keywords: Self-healing, cement, pelletisation, magnesium oxide, PVA coating.

1 Introduction:

Concrete outperforms other commonly used construction materials as a long-lasting and durable material. However, it is prone to cracking due to its limited tensile strength. The use of reinforcement can improve tensile load carrying capacity but cannot completely prevent crack formation. Although cracks are not considered as a damage, provided a prevailing crack width criterion is not exceeded, they are nevertheless undesirable. These cracks provide pathways for ingress of water, carbon dioxide, acid rain and other aggressive agents. The latter can not only induce corrosion of steel reinforcement but also degrade the concrete and accordingly the service life of reinforced concrete structures is shortened. In addition, cracks cause leakage in concrete structures, such as water reservoirs, roofs and water pipes, negatively affecting their functionality [1]. Thus, maintenance and repair work are essential and indispensable. The conventional repair methods increase the associated life-cycle cost of concrete structures, have a significant environmental impact and demand long and intensive labour. This led researchers to develop concrete that had a sufficient healing capability; cracks in concrete could be self-healed after cracking under specific conditions without any human intervention. This paved the way for infrastructures with reduced lifetime costs, improved durability and service life, both from an economic and environmental point of view [2], [3]

Cement based materials possess a certain capability to heal cracks intrinsically, which is called autogenous healing. This capability is mainly governed by chemical causes such as further hydration of cement grains and the formation of calcium carbonate [2], [4]. However, this autogenous healing is limited to microcracks (preferably less than 50µm) while the presence of water is essential [5], [6]. Using fibres can effectively improve the autogenous healing due to their capacity to control crack width and enhance multiple crack formation [7]. In an important step-forward, many researchers have explored the possibility of developing cement-based materials that heal autonomously. To achieve this, many techniques have been proposed such as

the addition of different mineral admixtures, bacterially induced carbonate precipitation, or using microcapsules or hollow fibres as carriers for healing agents.

The direct inclusion of mineral additives and admixtures in the concrete in small dosages has been reported in several studies [8]–[10]. Despite the capability of these minerals to produce more healing products to fill the cracking area, they face certain disadvantages such as: premature consumption and uncontrolled reactivity in contact with water when directly added in the mix - with other ingredients- without any protection [11]. Moreover in the case of expansive agents, expansion can occur in the interior matrix as well as in the cracked area, which could cause further cracking [1], [12]. Thus, researchers have suggested to envelope these minerals into capsules, glass tubes or coatings to be activated only at the time and location of cracking. For instance, Lee & Ryou [13] have investigated a coating encapsulation technique to envelope granulated calcium sulphoaluminate (CSA) into a polyvinyl alcohol (PVA) film. It was found that the PVA film coating could control the time of autonomic healing and prevented water migration via crack closing. Results also indicated an improvement of the healing efficiency of CSA in comparison with the direct application of healing agents in concrete without any coating. A recent study has also proposed to protect water soluble nutrients required for a special type of bacterial spore in a geopolymer coating [14]. Such coating will break whenever a crack occurs in the concrete matrix releasing the nutrients in the crack planes allowing the bacterial spores to germinate and precipitate calcium carbonate to heal the crack.

Three requirements need to be met in order to develop any encapsulation technique for self-healing of cement-based materials. Firstly, the encapsulation system should have compatibility and sufficient bonding with the concrete matrix. Secondly, it should be strong enough to preserve the sequestered healing compounds from unexpected events during the concrete mixing process, but brittle enough to rupture and release the healing agents when necessary. Thirdly, it should be chemically stable in the cement matrix, which is highly alkaline [14], [15]. The success of any system depends on the likelihood of two elements: (i) the crack path to coincide with the location

of the delivery system and (ii) the volume of healing agent to be released locally, since the latter is not ubiquitous in the matrix but concentrated at specific locations [16]. Similarly, the cargo material, in addition to promoting healing, has to disperse properly within the crack whilst having considerably extensive shelf life [16].

Three different powder minerals were examined in this study as core materials for the prototype pellets. A reactive magnesium oxide (MgO) was selected as the main potential self-healing agent in all formulations. MgO is an expansive mineral, able to yield irreversible and stable hydration products with compatible characteristics with the cement matrix [17]. Silica fume (SF), a silica-based additive was also tested for its potential to enhance self-healing. SF does not possess hydraulic behaviour by itself but can react with free $Ca(OH)_2$ and water, produced during the hydration of cement to form stable insoluble and densified calcium silicate hydrate (C-S-H) [18], [19]. Thus many researchers have proposed it for concrete repair and strengthening purposes [20], [21]. Bentonite (B) was also used as a dual-purpose material in some formulations. It is commonly used as a binder in the production of pellets [22], [23]. Bentonite has adequate binding properties throughout the temperature range of operation; it is also easy to handle, abundantly available, and inexpensive [23]. It can also play another significant role in filling cracks due to its high swelling capacity. It swells 15-18 times its dry size when wetted by water [24]. It is noteworthy here that all of the above minerals have good compatibility with the cementitious matrix.

Polyvinyl alcohol (PVA) was selected as the coating material for the pellets in this study because of its excellent chemical resistance, physical properties, low cost and ease of preparation [25]. As PVA is a water soluble substance, its films are easily prepared by a casting evaporation technique from aqueous polymer solutions, thus avoiding the use of organic solvents. The resultant films are clear, homogenous and resistant to tearing [26]. PVA is produced by the polymerisation of vinyl acetate to polyvinyl acetate, which is subsequently hydrolysed to PVA. The degree of hydrolysation represents the extent to which polyvinyl acetate has been hydrolysed

to produce PVA. Commercial PVAs are available as fully hydrolysed grades (degree of hydrolysis ≥98%) and partially hydrolysed grades (degree of hydrolysis ~86-89%) [27]. The solubility of PVA in water depends on the degree of hydrolysis and the degree of polymerization, with the effect of the former being especially significant. Some PVA grades with higher degrees of hydrolysis (>98%) are only soluble in hot water (50-100 °C); and form films that are insoluble in water at lower temperatures. In contrast, PVA grades with degrees of hydrolysis in the range of 75-98% are easily soluble in water. Molecular weight is another factor affecting the solubility of PVA and the extent of influence is related to the degree of hydrolysis. The solubility of highly hydrolysed PVA increases as the molecular weight decreases while the solubility of less hydrolysed PVA is relatively independent of molecular weight [26]. Thus, PVA with a high molecular weight and degree of hydrolysis of 98-98.8 % was used in this study.

This paper aims to provide the basic design and characterisation concepts of developed coated pellets as a self-healing system in cement based materials. To achieve this, pelletisation of potential powder self-healing agents was investigated in this study. Polymer film coating was then employed to envelope the formed pellets. The laboratory-developed pellets were compared with other types of pellets, which are commercially available.

2 Materials

2.1 Healing agents and coating material

Different magnesium oxide (MgO) based pellets were tested in this study. These included two types of commercial pellets (CP) in addition to different formulations of laboratory prepared pellets (prototype pellets, referred to as PP). The two CP types were LUVOMAG MgO pellets supplied by Lehmann & Voss, Germany, and MagChem, hard-burnt MgO pellets, supplied by Martin Marietta Magnesia Specialties, USA. For the PP, light-burnt MgO 92/200 (RBH, UK) was used. Silica fume (Elkem, UK) and bentonite clay (Macromin Kentish minerals, UK) were also utilised in different formulations of the prototype pellets. Magnesium oxide, silica fume and

bentonite are referred to as MgO, SF and B, respectively. The physical properties and chemical compositions of these materials are listed in **Table 1**.

Table 1: Chemical and physical properties of the pellet materials as provided by the suppliers

Chemical composition /properties		LUVOMAG Pellets	MagChem Pellets	MgO 92/200	Bentonite Clay	Silica fume
Chemical composition	CaO %	3.10	0.87	0.87	4.90	1.20
	SiO_2 %	2.47	2.25	2.25	54.20	93
	Al_2O_3 %	0.41	0.22	0.22	18.80	1
	Fe_2O_3 %	1.75	0.53	0.53	5.00	1
	MgO %	91.76	93.18	93.18	3.70	0.50
	SO_3 %	-	-	-	-	1
	Na_2O %	0.03	-	-	3.00	0.50
	TiO_2 %	0.03	-	-	0.70	-
	K_2O %	0.04	-	-	0.60	-
Properties	Loss on ignition LOI %	4.83	2.59	2.59	-	≤ 3
	Mean Particle Size (μm)	600-4750	75	75	4.75-75	≤ 45
	Particle density (g/cm^3)	-	3.02	3.02	2.8	-
	Surface area (m^2/g)	-	16.3	16.3	0.48	(15-30)
	Bulk density (g/cm^3)	-	-		-	200-350
	Reactivity* (sec)	283	4440	136	-	-

(*) Measured in the laboratory by the accelerated acidic test [28].

The developed pellets were protected by a coating shell. Polyvinyl alcohol (PVA) was used as the main coating material. PVA was obtained from Fisher Scientific as a 98-98.8% hydrolysed powder with an average molecular weight of 146,000-186,000g/mol.

2.2 Mortar mixtures

The cement used for the preparation of all mortar mixtures was CEM I (52.5N) with a particle density of 2.7-3.2g/cm^3 and a specific surface area of 0.30-0.40m^2/g, supplied by Hanson, UK. The chemical composition of the cement is presented in **Table 2**. Natural sand provided by a local supplier of building materials, Ridgeons, Cambridge, with 4mm maximum particle size was used in mortar mixes. All subsequent references to sand in this study refer specifically to this type of sand rather than natural sand in general.

Table 2: Chemical composition of cement as provided by the manufacturer

Materials	Composition (%)						
	CaO	SiO_2	Al_2O_3	Fe_2O_3	MgO	SO_3	LOI
Cement	63.60	19.50	4.90	3.10	0.90	3.30	2.10

3 Experimental procedure

3.1 Pelletisation process

The pelletisation process was conducted in a DP-14 "Agglo-Miser", a disc pelletiser supplied by Mars Mineral, USA. It is an inclined pan and variable angle and speed-pelletising device for laboratory or small production rate service. All pelletisation processes were conducted at ambient conditions of 20 ± 2°C and 50 ± 5% RH. First, the powder raw materials, MgO with SF or MgO with bentonite, were dry-mixed together using a cement paste mixer at the lowest speed for 3 minutes or until a homogenous blend was achieved by visual inspection. The dry mix was then loaded into the pelletiser drum wherein it was left to mix for 1 min ±5 sec. Subsequently, an appropriate quantity of tap water was uniformly added by a spray gun within 1 min ± 5 sec. **Figure 1a** shows the pelletisation process. During the process, the pelletiser was intermittently stopped to scrape the materials stuck to the pan and on the blades by a spatula. Thereafter, the formed pellets were dried in an oven at 60°C for one day. It is noteworthy to mention that various combinations of the selected pelletised powder materials with different water contents could be considered. However, as the number of possible proportions can increase infinitely, a preliminary stage was conducted to narrow down the number of trials. This was based on maximising the amount of self-healing agents and minimising the amount of water used as much as possible. Based on the preliminary investigations, two formulations were selected for this work: (1) MgO: B (1:1) with 30 % distilled water, and (2) SF: MgO (1:1) with 10% distilled water; all are by weight.

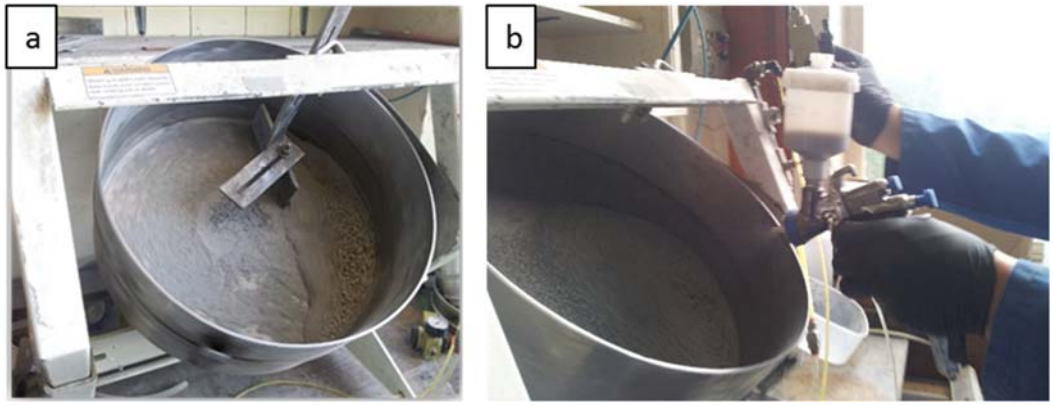

Figure 1: DP-14 "Agglo-Miser" pelletiser: (a) pelletisation process and (b) Spraying the coating solution on the pellets while the disc pelletiser rotates.

3.2 Coating process and characterisation

3.2.1 Preparation of the coating material

The coating solution was prepared by adding a pre-determined amount of PVA into distilled water which was allowed to hydrate overnight. The next day, the dispersion was slowly heated to 90°C ± 5°C while stirring at 700rpm until a homogeneous solution of 10% PVA was formed. The solution was then cooled to ambient temperature [29]. Water was added to compensate for any moisture loss that may have occurred during the heating process.

3.2.2 Coating process

The selected formulations of prototype pellets in addition to the commercial types of pellets were coated with the PVA based coating material. Each type was sorted into three groups upon size; 0.6-1mm, 1-2mm, and 2-4mm. The coating solution was applied in three layers to each group of pellets separately using a spray coating technique combined with simultaneous drying through a stream of hot air (60°C). During rotation of the disc pelletiser, pellets were sprayed with the coating solution as illustrated in **Figure 1b**. The coated pellets were then dried at room temperature for 48hrs and stored in an airtight plastic container until testing. Hereinafter, the coated prototype pellets are referred to as PP_MB and PP_SM for the formulations of MgO: B (1:1) and SF: MgO (1:1), respectively. The commercial coated pellets are referred to as CP_M1 and CP_M2 for LUVOMAG MgO and MagChem pellets, respectively.

3.2.3 Characterisation of the coating material

Three PVA solution samples, 20g each, were poured into a glass petri dishes (diameter 10cm) and oven-dried at 50 ± 2°C for 24hrs. The dried films were peeled from the petri dishes and stored in a desiccator at room temperature. The thickness of the films was measured by using a micrometre with 1μm accuracy. At least five thickness readings at different locations were taken for each test section and the results averaged. Thereafter, the PVA films were tested for specific properties to examine their suitability as encapsulation system for the healing materials according to the requirements discussed in the introduction.

3.2.3.1 Apparent solubility in water and in alkaline solution

To investigate the stability of the coating material in water, rectangular pieces (1x7cm^2) were cut from the PVA films and weighted. The dried pieces were immersed in distilled water for 24hrs; thereafter, the pieces were removed, spread on a clean petri dish and oven dried again at 50 ±2°C to a constant weight. The percentage weight loss, W%, expressed as the percentage of decrease in the weight of the film after immersion, represented the apparent solubility of the film. Five measurements were made and the average W% obtained [27].

In order to examine the survivability of the coating materials in the highly alkaline concrete environment, the PVA coating samples were immersed in a solution that simulated concrete pH conditions. For this purpose, a high pH solution (pH=12.5) was prepared, under continuous stirring, by dropwise addition of $Ca(OH)_2$ (10M) in distilled water.

3.2.3.2 Evaluation of the swelling properties

The swelling properties of the coating films were evaluated by using square pieces of the coating material of 1x1cm^2. The dimensions of each piece were accurately measured before immersion in distilled water for 5hrs. The pieces were then removed and spread on a clean petri dish. Accurate measurements of the dimensions were made immediately. The swelling index was defined as the percentage increase in the dimensions of the film after swelling [27]. Five pieces were made and the results averaged.

3.2.3.3 Water permeability

Three dried films were cut into circular sections with a diameter slightly larger than 4cm. The thickness of the tested films varied between 50µm and 100µm. Water permeability was measured using 4cm-diameter rounded polypropylene jars containing each 5gr of completely dried silica gel beads. These jars were capped by PVA films with different thicknesses and then stored at 25°C and > 95% RH for 24hrs. The weight of silica gel beads in each jar was recorded afterwards. The water permeability of the PVA films is calculated by the following formula [30]:

$$WP = \frac{\Delta m}{TS} \quad \textbf{(3)}$$

Where: WP is the water permeability ($g/m^2.h^{-1}$), Δm is the variation of the weight of silica gel beads (g), T is 24hrs and S is the cross-sectional area of the jar which equals $1.257x10^{-3}m^2$.

3.2.3.4 Dynamic Mechanical Analysis (DMA)

DMA analysis was performed using a DMA 8000 (Perkin Elmer, UK), in tensile mode, at a frequency of 1Hz, and by heating from 0°C to 100°C at a rate of 5°C/min in a nitrogen atmosphere. Strips with dimensions of about $6x10x0.25mm^3$ were subjected to a sinusoidal deformation of 5mm amplitude. The test was conducted on strips in three conditions: (1) dried, (2) immersed in water for 24hrs and then dehydrated in the oven at 50 ± 2°C to a constant weight and (3) immersed in alkaline solution for 24hrs and then dehydrated in the oven at 50 ± 2°C to a constant weight.

3.2.3.5 Measurement of coating thickness

Ten pellets were taken randomly from each group of the coated pellets to measure their coating thickness using scanning electron microscopy SEM-PHENOM PRO.

3.3 Characterisation of pellets

The particle size distribution of the coated pellets was assessed by a set of sieves ranging from 75µm to 20mm and an automatic sieve shaker (Controls, UK). A pycnometer method was chosen for determination of the true density (ρ_a) of pellets using ethanol (95%) as an immersion fluid

[31]. The bulk density (ρ_b), which is the mass of pellets divided by the volume including the pore volume, was also determined by the pycnometer. The porosity is thus calculated using **Eq 1** [32]:

$$Porosity = [1 - \left(\frac{\rho_b}{\rho_a}\right)]\% \quad \textbf{(1)}$$

Pellet crushing strength was measured for both uncoated and coated pellets by a semi-automatic hardness tester (TH3, 500N). At least 20 pellets in the size range of 2-4mm of each type of the pellets were tested to establish crushing strength and the mean value was adopted. In addition, the shape factor ($\varphi_{circularity}$) also called circularity, reported by [33] was used to evaluate the pellets shape. Pellets of different sizes (minimum 20) were placed on a flat surface on their most stable plane to produce the largest projection area. The shape factor is then calculated as follows:

$$\varphi_{circularity} = \frac{4.\pi.A}{P_{rough}^2} \quad \textbf{(2)}$$

where (A) is the projected area of the pellet and P_{rough} is the perimeter of the projection. Due to the incorporation of the overall perimeter, this shape factor takes into account the roughness of pellets in addition to the shape. Microscope images of pellets on the largest projection area were taken and the perimeter was measured counting all pixels of the pellet outline. Measurements were carried out using image analysis software (Image-J). Shape factor values can range from zero to one, where one represents a perfect spherical shape.

3.4 Survivability and compatibility studies:

3.4.1 Mechanical properties and distribution:

Ten mortar mixes with water-to-cement ratio (w/c) of 0.5 and sand to cement ratio of 3:1 were prepared for this study as presented in **Table 3**. The developed self-healing pellets (SHP) were incorporated as a partial replacement of sand for all mixes except for the control mix. All specimens were demoulded after 1 day and then cured in a water tank at a temperature of 20 ±2°C until the desired testing age. For each mix, 12 cube specimens (40x40x40 mm^3) were prepared in order to investigate the influence of pellets on the mechanical properties of mortar specimens. Two cylinders of Ø100x50mm were also cast for investigating the distribution of

pellets inside the concrete matrix. The cylindrical specimens were sawn into 15 mm thick discs and the middle discs from each specimen were extracted and photographed.

Table 3: Compositions of mortar mixes by percentage weights

Mix ID	Mix ingredients fractions by weight (%)				SHP used	
	Portland Cement	Water	Natural sand	SHP	Type	Size (mm)
M1	22.2	11.1	66.7	-	-	-
M2			60	6.7	PP_MB	1-2
M3					PP_MB	2-4
M4					PP_SM	1-2
M5					CP_M1	0.6-1
M6					CP_M1	1-2
M7					CP_M1	2-4
M8					CP_M2	1-2
M9			63.35	3.35	PP_MB	1-2
M10			53.3	13.4	PP_MB	1-2

3.4.2 Workability

To determine the effect of adding the pellets on the flow and consistency characteristics of the fresh mortars, a flow table test was conducted according to BS EN 1015-3:1999. The truncated conical mould (larger base at the bottom) with its funnel was set centrally on the disc of the flow table. The mortar was introduced into the mould in two layers, each layer being compacted by at least 10 short strokes of the tamper to ensure uniform filling of the mould. The excess mortar was then skimmed off with a palette knife and the disc was carefully cleaned of any paste or water. After 15 seconds, the mould was lifted vertically and the disc was jolted 15 times at a constant frequency of one per second to spread out the paste. The diameter of the paste spread was measured in two directions at right angles and the average was stated to the nearest mm. The test was replicated.

3.4.3 Isothermal calorimetry test

A Calmetrix I-Cal 2000 high precision isothermal calorimeter compliant with ASTM C1679 was used to evaluate the effect of pellet additions on the hydration process of the different mortar mixes. The test was replicated for each mix. The instrument functions by measuring the heat

flow required to maintain isothermal conditions, recorded in watts. When this data is normalized by the mass of the sample used, the changes in heat evolution in the binder can be measured. The thermostat of the calorimeter was set to 23 °C and left to stabilise for 24hrs. Pre-conditioning of the cement, sand, pellets, and water took place for 2hrs before being mixed for one minute using a plastic spoon. The quantities of cement, sand and water used were 15g, 30g and 12g, respectively and pellets replaced sand by 10% of weight. The heat of hydration and the cumulative heat production was then recorded for the first 48hrs. This time was sufficient to obtain the initial setting peak. The peak power is calculated as the maximum power (first peak) minus the power during the induction period (first trough). The initial setting time was then calculated as the time at one-third of the peak power.

3.4.4 Unconfined compressive strength

The compressive strength testing was carried out using Controls Advantest 9 with a maximum capacity of 250kN and a loading rate of 2400 N/s. Triplicate cubes were tested at ages of 7, 28, 56 and 90 days and the strength reported was an average of the three specimens.

4 Results and discussion

4.1 Characterisation of the PVA coating

An overview of the main characteristics of the PVA coating material used in this work is given in **Table 4**. Through visual observations, it is evident that PVA films were clear, non-tacky, homogenous, tough and glassy at room temperature, but turned into rubbery films in the presence of water at room temperature. Nevertheless, they retained their integrity in water and in high alkaline solution. They were slightly soluble in water (11%) and less soluble in high pH solution. These results are in accordance with Chan et al. (1999). The authors showed that PVA with a degree of hydrolysis of 99.45% and a molecular weight of 140,000-150,000g/mol exhibited apparent solubility of 15.5 ±3.4% after 24hrs immersion in water at room temperature. In general, the amount of material which may be extracted by water from any polymer film depends on its chemical nature, the temperature of water, the length of the polymer chain and the time of

immersion in water [34]. Thus, a possible explanation for the weight reduction in PVA films might be that the hydroxyl groups in the polymer interact with water molecules through hydrogen bonds. Since the PVA used, has a high degree of hydrolysis and molecular weight, strong intermolecular and intramolecular hydrogen bonds were formed via hydroxyl groups between molecules of PVA. This reduced the extent of interaction between PVA and water molecules, resulting in lower solubility in water [27], [35]. The further reduction of solubility in high pH solution could be due to the decrease in free hydrogen ions in the water solution that could react with the hydroxyl groups in PVA [36], [37].

Results also showed that the swelling index of the PVA films varied from 30% to 45% (**Table 4**). The thickness of the tested films varied between 100µm and 250µm. As the amount of PVA increased and accordingly the thickness of the film increased, the swelling index decreased. Given that the PVA molecule has both crystalline and amorphous regions, the swelling of PVA films will be governed by both the degree of crystallinity and the average chain length in the amorphous region of the film. Increasing the degree of crystallinity by increasing the amount of PVA in the produced films decreases the swelling [38].

Table 4: Characteristics of the PVA coating material

Parameter	Average value
The percentage weight loss W% in water	11 % (SD = 2.22)
The percentage weight loss W% in alkaline environment	4% (SD = 0.67)
Swelling index (%)	30% - 45% (depends on the thickness of the film)
Water permeability (WP) ($g/m^2.h^{-1}$)	~ zero

SD: standard deviation

With DMA, the sample was subjected to an oscillatory stress and the material response was measured. The nature of this response was used to determine the elastic and viscous properties of the material; storage modulus and phase angle (tan delta). DMA thermographs, shown in **Figure 2**, present the storage modulus and the phase angle (tan delta) as a function of the dynamic force. These graphs illustrate the effect of water and the high alkaline solution on the mechanical behaviour of the coating material.

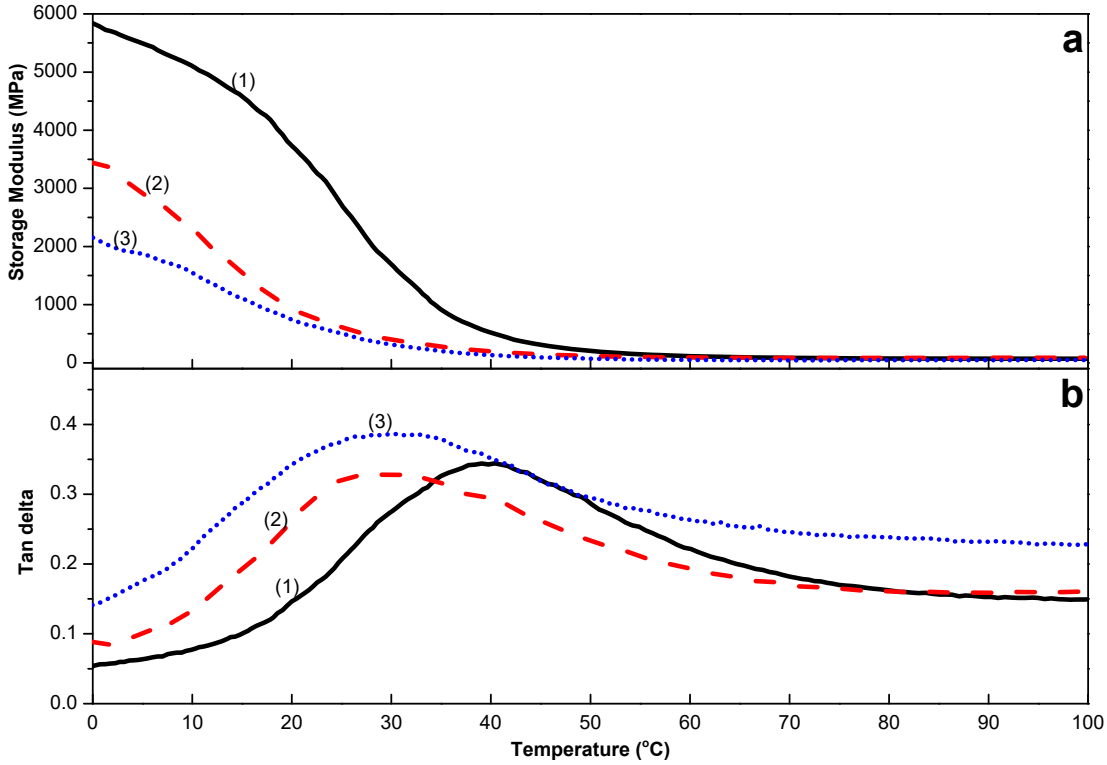

Figure 2: (a) storage modulus and (b) tan delta (the ratio between the loss modulus and the storage modulus) for: (1) dried PVA film, (2) dehydrated PVA film after immersion in high pH solution and (3) dehydrated PVA film after immersion in water.

The storage modulus is a measure of the elastic energy stored during deformation [39]. Results showed a decrease in the storage modulus of the PVA sample when immersed in water or high pH solution. At room temperature (20± 2°C), the storage modulus was about 3670MPa and it reduced to 911MPa and 723MPa after immersion in high pH solution and water, respectively.

Figure 2b shows the change of tan delta with temperature and from this plot the glass transition temperature (T_g) is calculated as the peak of the tangent delta signal. Tan delta is defined as the ratio between the loss modulus and the storage modulus and represents the relative contribution of the viscous versus elastic properties [39]. The glass transition temperature is defined as the point at which a material changes from a stiff, "glassy" state to a softer, more "rubbery" state. Physically, it is the point at which polymer chains gain enough energy in order to substantially increase their mobility within the polymer matrix and this is reflected in a sharp change in

material flexibility and an increase in the sample's heat capacity. From the tan delta graph (**Figure 2b**), it is observed that the immersion of PVA samples in water or a high pH solution shifted $T_g$to lower temperatures. T_g exhibited a decrease from 39°C when tested as a dried sample to 27°C and 28.7°C when tested after dehydration from a high pH solution and water, respectively. This can be attributed to the interaction of some PVA hydroxyl groups with water molecules through hydrogen bonds and thus reduced the stiffness of the PVA sample [25]. Although PVA films exhibited a decrease in their mechanical properties in water or high pH solutions, as expected for a water-soluble material, they maintained integrity and stability, which meets the desired requirements here.

4.2 Characterisation of the pellets

Figure 3 shows samples of each type of pellets used in this study; they are categorised in three different size groups. **Figure 4** compares the particle size distributions (PSD) of PP_MB, PP_SM, and CP_M1 pellets with respect to the PSD of the sand. The CP_M2 pellets are excluded herein as they were provided from the manufacturer as batches with sorted sizes; 0.6-1 mm, 1-2 mm or 2-4 mm. The PSD curves indicate that the size distribution of the three types of pellets was close to the size distribution of the sand with a slight shift towards greater particle size for the PP_MB, and CP_M1 while PSD of PP_SM pellet shifted towards smaller particle sizes. As shown in **Table 4**, D_{50} of PP_MB, PP_SM, CP_M1, and sand were 1.2mm, 0.35mm, 1.35mm, and 0.47mm, respectively. It is noteworthy here that ≤10% of the two types of PP are exceeded 4 mm; this couldn't be entirely controlled in the pelletisation process.

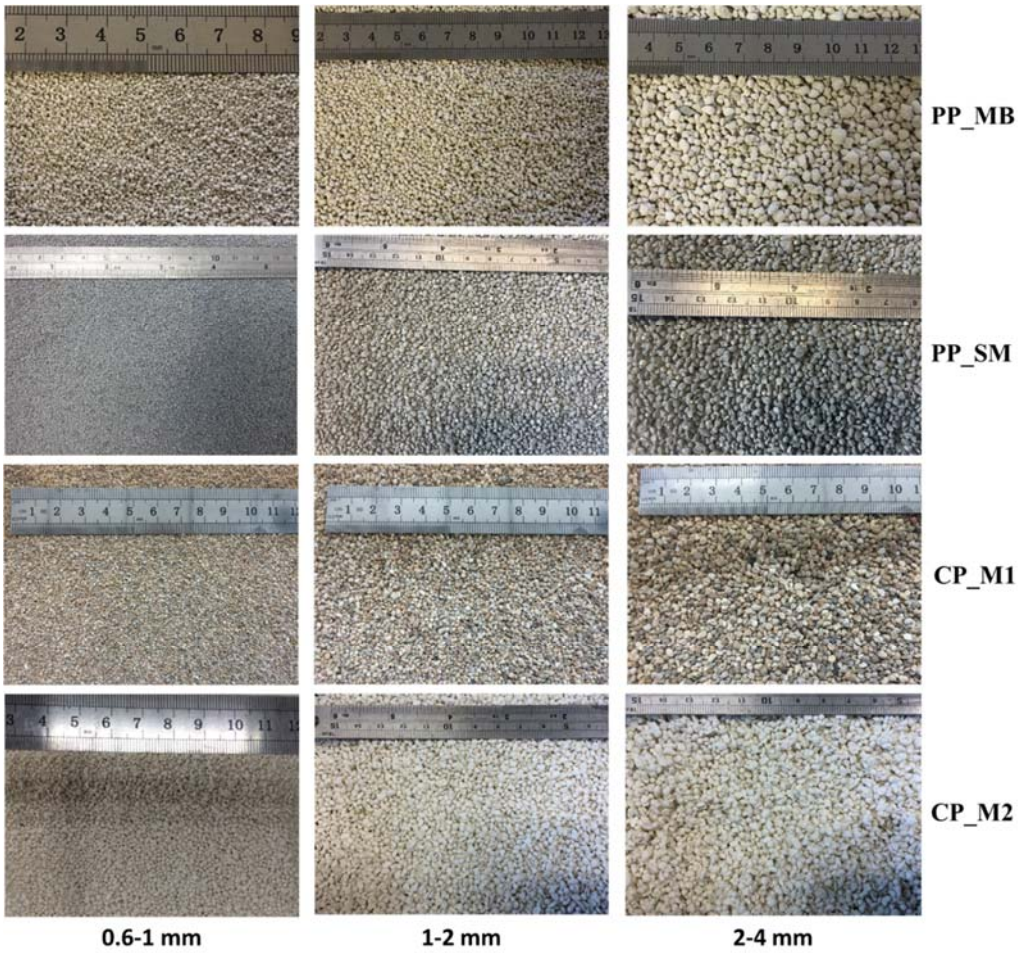

Figure 3: Samples of different types of the coated PP and CP pellets categorised according to the size.

The various geometrical and physical properties of the different types of pellets and sand are presented in **Table 5**. The coefficient of uniformity (C_u) and the coefficient of curvature (C_c) for pellets and sand are demonstrated. C_u is an important shape parameter indicating how wide the range of the particle sizes is as well as describing the slope of the PSD curve. Thus, a high C_u value indicates a wide range of particle sizes. C_c is another shape parameter describing the grading of the particle. Holtz and Kovacs (1981) proposed that for a sand to be classified as well graded, the following criteria should be met: $C_u \geq 6$ and $1 < C_c < 3$. These criteria were applied to both the PP and CP pellets for their characterisation. C_u values for both PP pellets are > 6. In contrast, C_u of CP-M1 pellets is less than 6. C_c values of both PP_MB and CP_M1 are between

1 and 3 but C_c of PP_SM is less than 1. This indicates that among all types, PP_MB are the most well graded pellets.

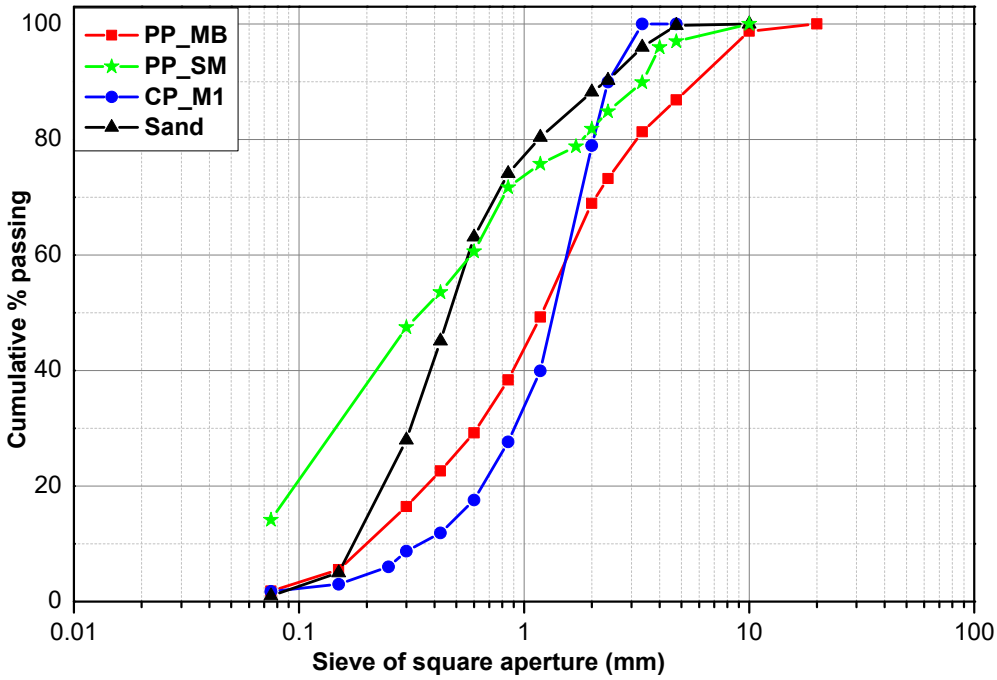

Figure 4: PSD of PP_MB, PP_SM and CP_M1 pellets compared to the PSD of sand.

In addition, it would be useful to consider what the data reveal about the porosity and density of PP and CP pellets. These results, in comparison with sand, are presented **Table 5**. All pellets exhibited lower bulk densities and greater porosities than those for sand. The bulk density of pellets was between 0.95-1.54g/cm^3 whereas it was 2.05g/cm^3 for sand. This denotes that the replacement of sand by the same weight of pellets in any concrete mix will increase the occupied volume by 33% to 115% according to the pellet type. PP_MB, CP_M1 and CP_M2 pellets exhibited very close porosity values (61.2%, 60% and 58.9%, respectively). In contrast, the porosity of PP_SM was much lower (45.2%). This could be attributed to the particle size of SF (≤ 45 µm) while the particle size of the MgO is ~75 µm. Accordingly, the presence of SF in the formulation, results in less inter-particle voids

Table 5: Properties of PP and CP pellets in comparison with sand particles

Parameter	PP_MB	PP_SM	CP_M1	CP_M2	Sand
D_{50}	1.2	0.35	1.35	-	0.47
Coefficient of uniformity $C_u = \frac{D_{60}}{D_{10}}$	7.8	7.65	4.7	-	3.3
Coefficient of curvature $C_c = \frac{D_{30}^2}{D_{60} \times D_{10}}$	1.24	0.48	1.62	-	1.02
Oven bulk density (g/cm^3)	0.95	1.59	1.3	1.54	2.05
Particle density (g/cm^3)	2.45	2.9	3.25	3.75	3.33
Porosity (%)	61.2	45.2	60	58.9	38.4

The circularity factor was adopted here as it takes into consideration not only the shape of pellets but also the roughness of surfaces. **Figure 5** presents the shape factor values with the standard deviations for all pellet types compared to sand. All values of the pellets were in the range of 0.81 to 0.86 while the value of sand was 0.79. This indicates that PP and CP were partly rounded and slightly more circular than sand particles.

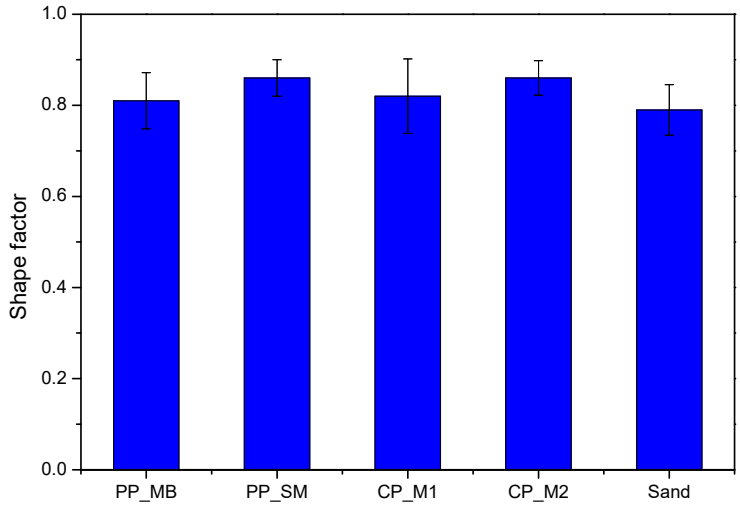

Figure 5: Shape factor ($\varphi_{circularity}$) of the different type of pellets in comparison with sand.

Taken PSD, density, porosity and shape properties together, the prototype pellets showed comparable mechanical and physical properties to the commercial pellets and sand. Therefore, it could be concluded here that the selected powdery healing agents were successfully converted into pellets.

When the PVA solution was sprayed on the pellets while they were tumbling in the pan of the disc pelletiser, it formed a thin film on the surface of the pellets. In order to obtain a complete coating, covering all the surface of the pellet, at least three cycles of spraying of the PVA solution were required. SEM images in **Figure 6** show the PVA coating of an individually coated pellet after three cycles of spraying the coating material. The thickness of the PVA shell varied between 10µm and 50µm.

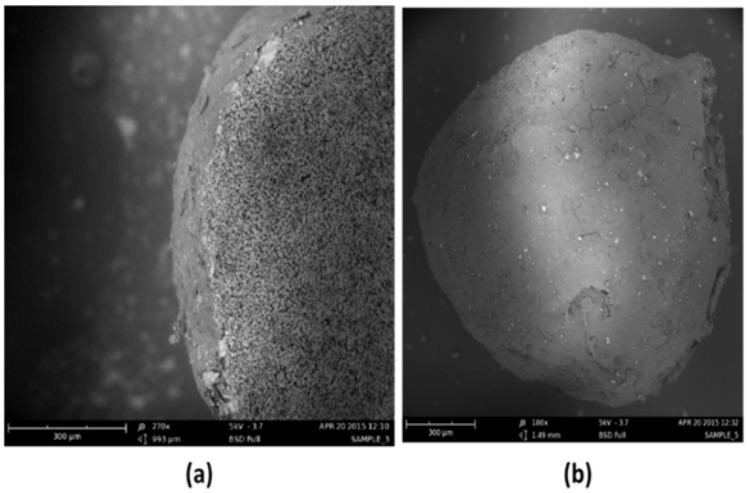

Figure 6: Cross-section scanning electron microscope (SEM) of the film-coated pellets: (a) the thickness of the PVA coating for individual pellet, and (b) the surface of a pellet completely covered by the PVA coating.

In addition, crushing strength tests for uncoated and coated CP and PP pellets were performed for pellets with 2-4mm size, from each type. This size was selected in compliance with the range of hardness testing equipment used. **Figure 7** illustrates the average crushing strength values with the standard deviations of all pellet types. The average crushing strength of PP_MB and PP_SM uncoated pellets were 7.4N and 9.5N; these values increased to15.2N and 11N after coating, respectively. While CP_M1 and CP_M2 showed a strength of 11.3N and 38N before coating respectively, they both gained more strength after coating (24.4N and 41N). It could be inferred here that there is a direct correlation between the strength and the porosity values shown above**.** An increase of the former accompanies a decrease in the values of the latter. Results indicated that the coating increased the pellet crushing strength between 15% and 105%. However, this is a wide range and could not be translated to an empirical relation. Moreover, this

could be attributed to the variability of the coating thickness (10-50µm), which was not controlled in this work. However, none of the crushing strength values of the coated PP and CP exceeded 33% of the sand particles crushing strength. This is favourable as the pellets are expected to rupture when a crack occurs provided that they survive first the concrete mixing. Yet, none of the previous research has dealt with specific values for the required strength to meet these requirements.

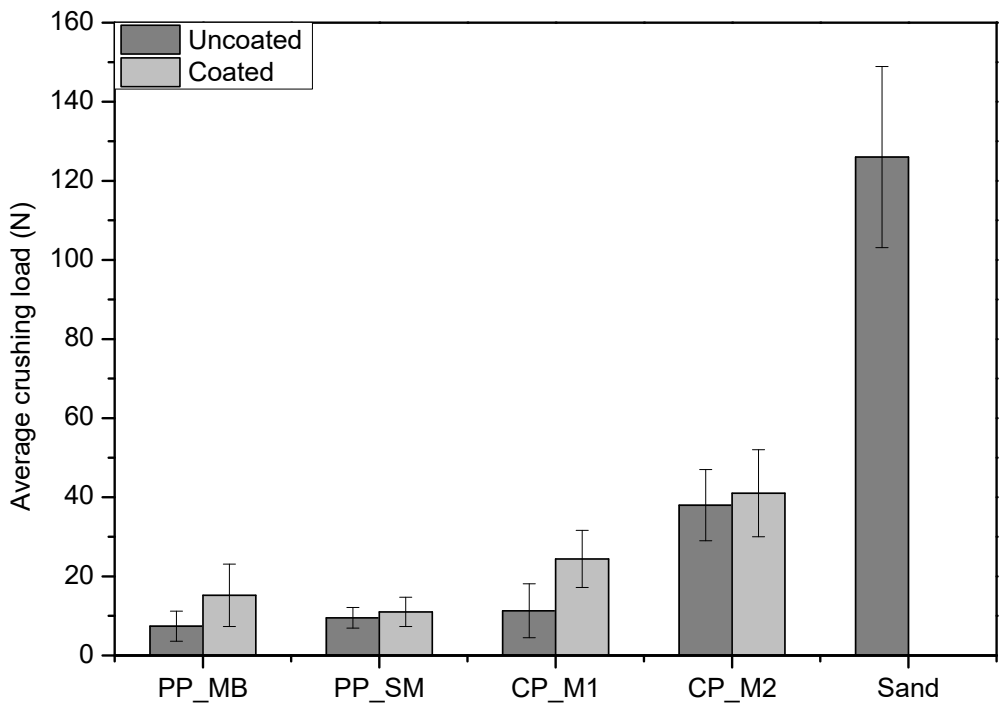

Figure 7: Average crushing strength values of different types of pellets compared to sand

4.3 Influence of pellets on the properties of the mortar mixtures

4.3.1 Flowability of the fresh mixes

Figure 8 illustrates the influence of different types of pellets on the flow values. The control mix (M1) showed a flow value of 156mm; this was reduced to 142.5mm, 129mm, 152mm, and 155mm for M2, M4, M6 and M8 mixes, respectively. The addition of CP had a lower influence on the flow values compared to the addition of PP, leading to a noticeable decrease in the flow values. The latter effect was more pronounced in M4 with PP_SM; with a flow value which was reduced by 17%. The change in pellet weight fraction also affected the workability of the mix. As **Figure 8b** shows, when the PP_MB fraction increased, the flow value decreased. Results

indicate that the addition of 5% of PP_MB had a negligible influence on the flowability of the mortar mix. In contrast, the addition of 10% and 15% of PP_MB decreased the flow value by ~10% and 18%, respectively.

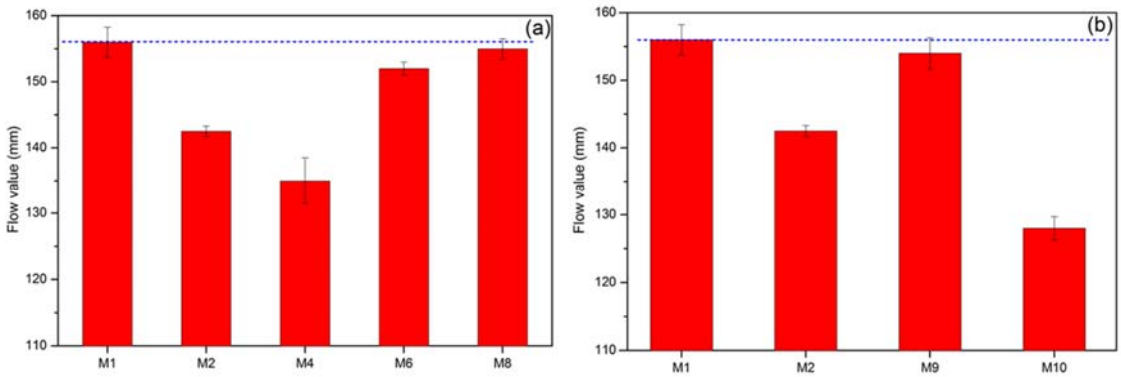

Figure 8: The flow table values for mortar mixes with: (a) different type of pellets and (b) different proportions of PP_MB pellets, compared to the control mix.

There are two possible explanations for these results. Firstly, since the pellets have lower densities when they partially replace sand by weight they lead to an increase of the occupied volume of sand by 33% to 115% according to the pellet type as discussed above in **section 4.2** Thus, the sand/ cement ratio by volume increased in the case of any SHP/ sand replacement, and this subsequently decreased the cement quantity available per unit volume of the mix. Cement content affects the workability of concrete; the larger the quantity of cement, the greater the volume of paste available to coat the surface of aggregates and fill the voids between them. This will help to reduce the friction between aggregates and smooth movement of aggregates during mixing and thus increasing the workability of concrete [41], [42]. Secondly, as discussed previously, the crushing strength of all SHP did not exceed 30% of sand. It is possible, therefore, that a proportion of the added pellets could not survive the mixing. This could imply that the cargo materials of the crushed pellets may have contributed to the hydration process from the beginning consuming some water and accordingly reducing the workability of the mix.

In the case of PP_SM, any broken-down pellets would release SF and MgO into the mix. The water demand of concrete containing silica fume, increases with increasing amount of silica fume. This increase is caused primarily by the high surface area of the silica fume [43], [44].

Thus, the effect of adding PP_SM on the workability was more pronounced compared to the other SHP.

The effect of pellet size on the workability of the fresh mixes was also investigated. The general trend in **Figure 9** shows that an increase in pellet size led to a workability reduction. This could be due to the amount of released cargo materials that can contribute to the hydration process from the mixing process as some pellets do not survive this. In the case of larger pellet sizes, broken-down pellets would yield larger amounts of inner materials that react early in the concrete matrix. The latter effect becomes less prominent with smaller sizes. However, this trend is not valid in the case of M6 where the increase of pellet size from 0.6-1mm to 1-2mm resulted in an increase of flow values from 146mm to 152mm. Nevertheless, all mortar mixes exhibited sufficient workability to be mixed, compacted and cast properly.

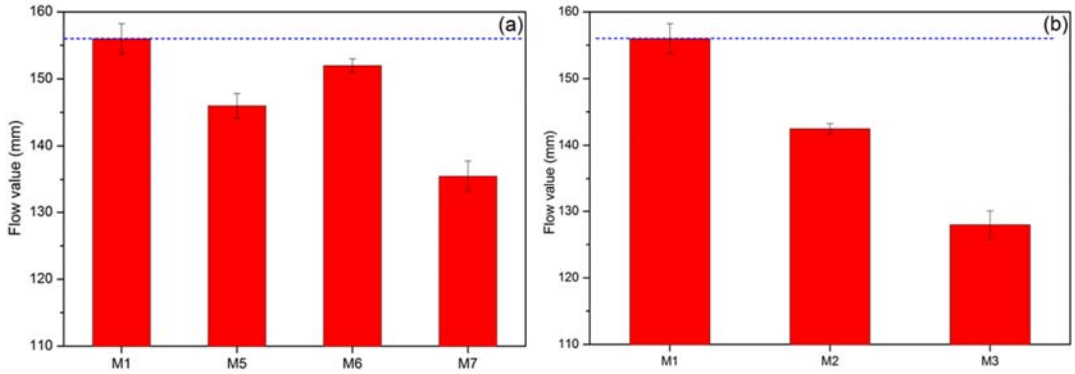

Figure 9: The flow table values for mortar mixes with different sizes of: (a) CP_M1and (b) PP_MB, compared to the control mix.

These results are in good agreement with those obtained by Hung and Kishi (2013). They studied the workability of fresh concrete containing granules of supplementary cementitious materials. The input of self-healing granules into the concrete mix caused a slight decrease in workability and accordingly increased the needed amount of superplasticiser compared to that in plain concrete. They attributed this to the water absorption and further reaction between the coating layer of granule and the mixing water. However, they concluded that granules could be considered as an effective approach to overcome the drawbacks of direct incorporation of healing materials in a powder form such as the reduction of workability.

4.3.2 Calorimetry

The power and cumulative energy produced per gram of cement for the first 48hrs for mixes containing different SHP and their uncoated counterparts, in comparison to the control mix, are shown in **Figure 10** and **Figure 11**. In addition, setting time and peak power values for all mixes are summarised in **Table 6**.

Generally, it can be seen that the addition of coated pellets showed a slight variation in the setting time and peak power values compared to the control mix. The initial setting time was not affected by the addition of PP_MB or CP_M1 whereas PP_SM reduced it slightly (from 3.8 to 3.7) and CP_M2 increased it to 3.9hrs. In contrast, the addition of uncoated pellets caused a remarkable change in the setting time. PP_MB and CP_M1 increased the setting time from 3.8hrs to 4.1 hrs while CP_M2 accelerated the setting time (3.4hrs).

Similarly, the peak power was only slightly affected by the addition of coated pellets. For example, it decreased by ~ 9% in the case of adding PP_MB while it increased by 10%, 7.5% and 15.6% when adding PP_SM, CP_M1 and CP_M2, respectively. On the contrary, the change in the peak power was more pronounced in the case of uncoated pellets. As **Table 6** illustrates, the addition of uncoated pellets increased the peak power in the range of 15% and 40%.

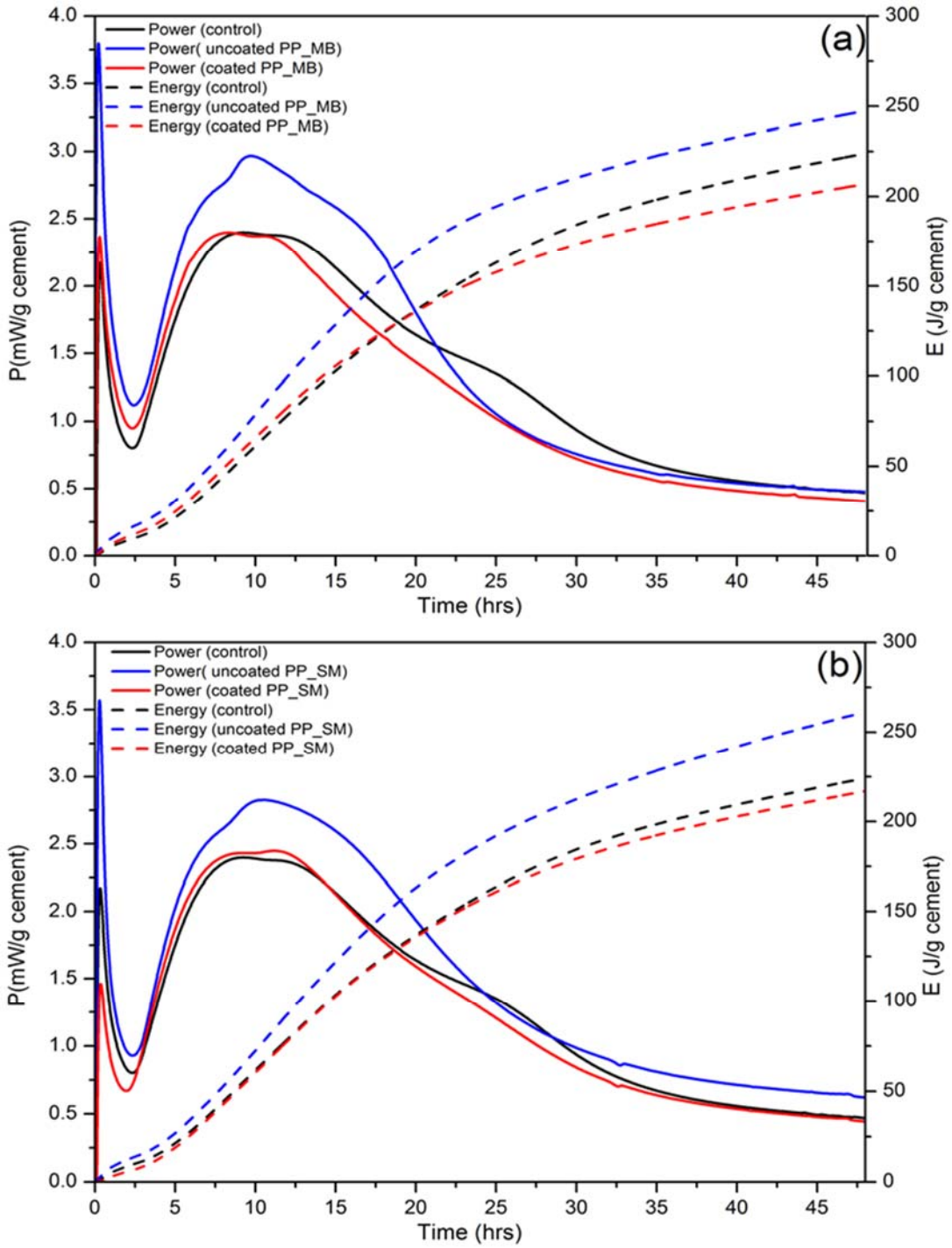

Figure 10: Effect of pellet addition on isothermal (23°C) power and energy production of mortar mixes: (a) coated and uncoated PP_MB and (b) coated and uncoated PP_SM.

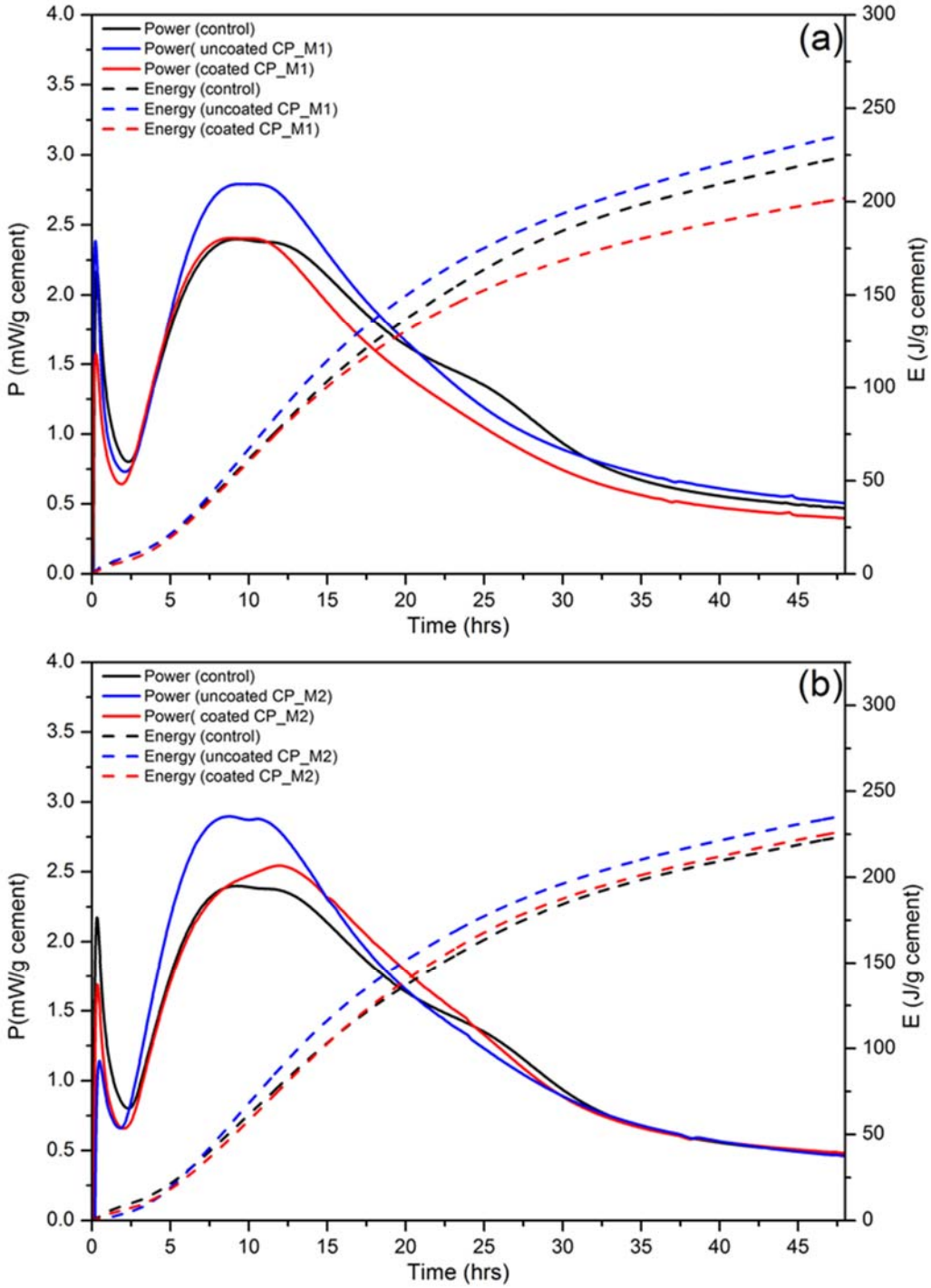

Figure 11: Effect of pellet addition on isothermal (23 ºC) power and energy production of mortar mixes: (a) coated and uncoated CP_M1 and (b) coated and uncoated CP_M2.

Table 6: Initial setting time and peak power values for mortar mixes containing pellets compared with the control

The type of pellets in the mix	Initial setting time (hrs)	Peak power (mW/g)
Control	3.8	1.6
Coated (PP_MB)	3.8	1.48
Uncoated (PP_MB)	4.1	1.83
Coated (PP_SM)	3.7	1.76
Uncoated (PP_SM)	3.9	1.91
Coated(CP_M1)	3.8	1.72
Uncoated (CP_M1)	4.1	2.08
Coated (CP-M2)	3.9	1.85
Uncoated (CP-M2)	3.4	2.2

This difference in the effect of coated and uncoated pellets on the setting time and peak flow of fresh mixes confirms the efficiency of enclosing pellets into the coating. For the mixes containing the coated pellets, the small differences in the setting times and peak power values compared to the control are not necessarily due to the rupture or breakage of coating during mixing: it could be attributed to the change in the volume. The pellets occupied more volume than the sand, which may have disturbed the hydration of cement or at least provided bigger volume to dissipate the exothermal heat.

4.3.3 Distribution of pellets inside mortar matrix

In order to explore the distribution of pellets inside the mortar specimens, sliced discs were taken from the middle of the cast cylinders. **Figure 12** shows the distribution of PP_MB and CP_M1 pellets across the sample sections. Some white (**Figure 12a**) and off white (**Figure 12b**) semi-round dots can be seen indicating PP_MB and CP_M1 pellets, respectively, adhered to the cement or sand particles. Both types of pellets were distributed all over the mortar matrix and did not exhibit any agglomeration.

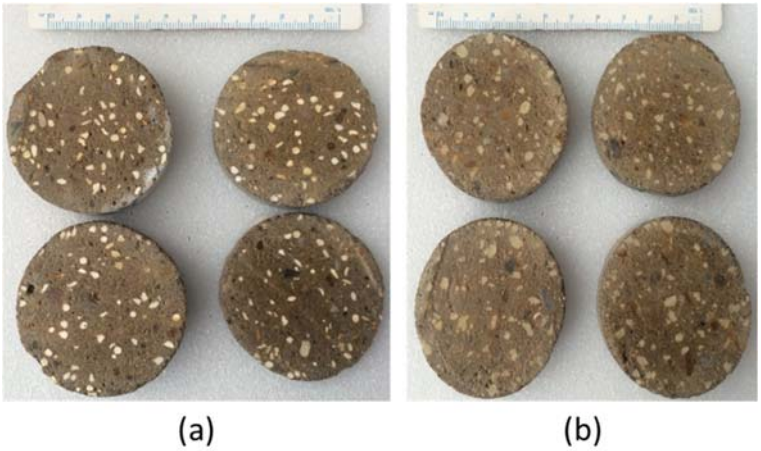

Figure 12: Characteristic disc sections showing the distribution of pellets inside the mortar specimens: (a) PP_MB pellets, and (b) CP_M1 pellets.

In addition, it was found that the pellets had a good bonding with the cementitious matrix as shown in **Figure 13**. This could be attributed to the hydrophilic nature of PVA, which enhances the bonding between the PVA shell and the cementitious matrix. This behaviour has been identified in PVA based fibres used in cementitious composites increasing their popularity throughout the world [46], [47]. The improved mechanical interlock of PVA to the cementitious matrix can be attributed to the hydroxyl groups on the carbon backbone which attract the water molecules and consequently result in to strong hydrophilic characteristics [48], [49].

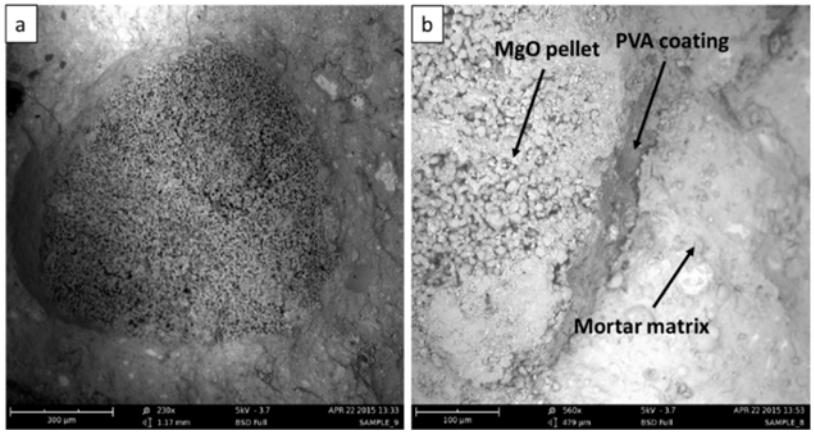

Figure 13: SEM images of PP_MB pellet in the cementitious matrix.

4.3.4 Unconfined compressive strength (UCS) development

The UCS values of mortar cube specimens at different ages (7, 28, 56 and 90 days) with their standard deviations are presented in **Figure 14** and **Figure 15**. In terms of SHP type, it can be

seen from **Figure 14a** that M1, M2, M6 and M8 specimens demonstrated constant strength gain with time. In contrast, M4 showed a significant increase from 18MPa at 7 days to 37MPa at 28 days and afterwards matched the other mixes. Generally, the replacement of sand by any SHP reduced the compressive strength. Nevertheless, M4 and M6 exhibited values very close to the control. The deviation did not exceed 10% at any age except for M4 at 7 days (~ 40%). Nonetheless at later ages (90 days), M4 displayed higher strength; namely, 45.7MPa compared to 44.2MPa for the reference. Conversely, M2 and M8 showed a remarkable reduction in compressive strength. The latter is more pronounced in the case of M8. Compared to the control, the decrease of the average compressive strength of M2 and M8 reached 14% and 25% at 28 days and ~12 % and 15% at 90 days, respectively. The displayed reduction could be due to three reasons. Firstly, the difference in crushing strength between SHP and sand particles as illustrated above in **Figure 7**. Secondly, the partial replacement of sand by SHP increased its volume and accordingly decreased the cement and water proportions in terms of specific volume, resulting in a reduction of the compressive strength. Thirdly, the possible breakage of some pellets in the mortar matrix could have released the cargo materials from the crushed pellets. These can contribute in the hydration process; however, their effect varies according to the type and reactivity of these materials.

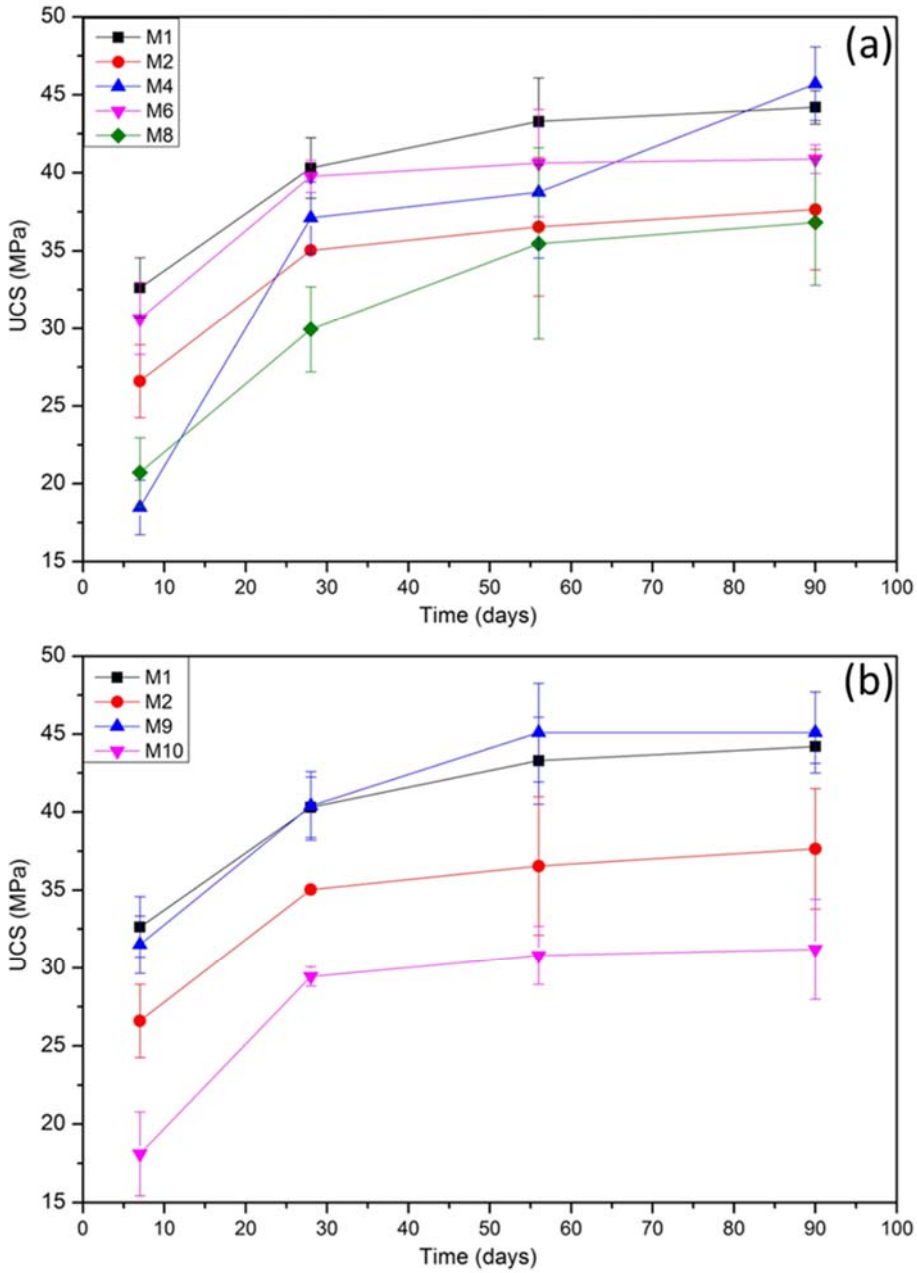

Figure 14: UCS of mortar samples containing: (a) different pellet types at different ages, and (b) different proportions of PP_MB at different ages.

The effect of changing the weight fraction of the added PP_MB is shown in **Figure 15b**. There is a clear trend of decreasing compressive strength with increasing weight fraction of pellets. M9 containing 5% of pellets showed negligible differences in strength values compared to the control at all ages. Increasing the pellet fraction to 10% by weight resulted in a reduction of ~ 8% of the compressive strength at all ages. Increasing the replacement of sand by PP_MB to 20% by weight led to a detrimental decrease (~ 30%) in the strength values at all ages.

On the other hand, it is clear from **Figure 15**, that there is a pronounced descending trend in the UCS values of the mortar samples with the increase of pellet size. For instance, it was observed that the strength values of CP_M1 pellets at 28 days decreased from 40.28MPa for M5 with 0.6-1mm pellets to 39.8 and 37.3MPa for M6 and M7 with pellets of size 1-2mm and 2-4mm, respectively (**Figure 15a**). Similarly, when PP_MB size increased from 1-2mm in M2 to 2-4mm in M3, the average strength values decreased from 35MPa to 24.8MPa at 28 days and from 37.65MPa to 32.1MPa at 90 days. However, the reduction in UCS values was more obvious in the case of PP_MB when compared to CP_M1.

Overall, it could be concluded here that the addition of SHP reduced the compressive strength values. However, up to 10% replacement of sand, the reduction did not exceed 15%, which corresponds to the literature. For instance, Pelletier et al. (2011) reported that the addition of 2% volume of microcapsules with a diameter up to 800µm decreased the compressive strength by 12-15%. Hung & Kishi (2013) also showed that the reduction of compressive strength due to the addition of self-healing granules varied between 2% and 13% at 28 days and 3% and 19% at 91 days.

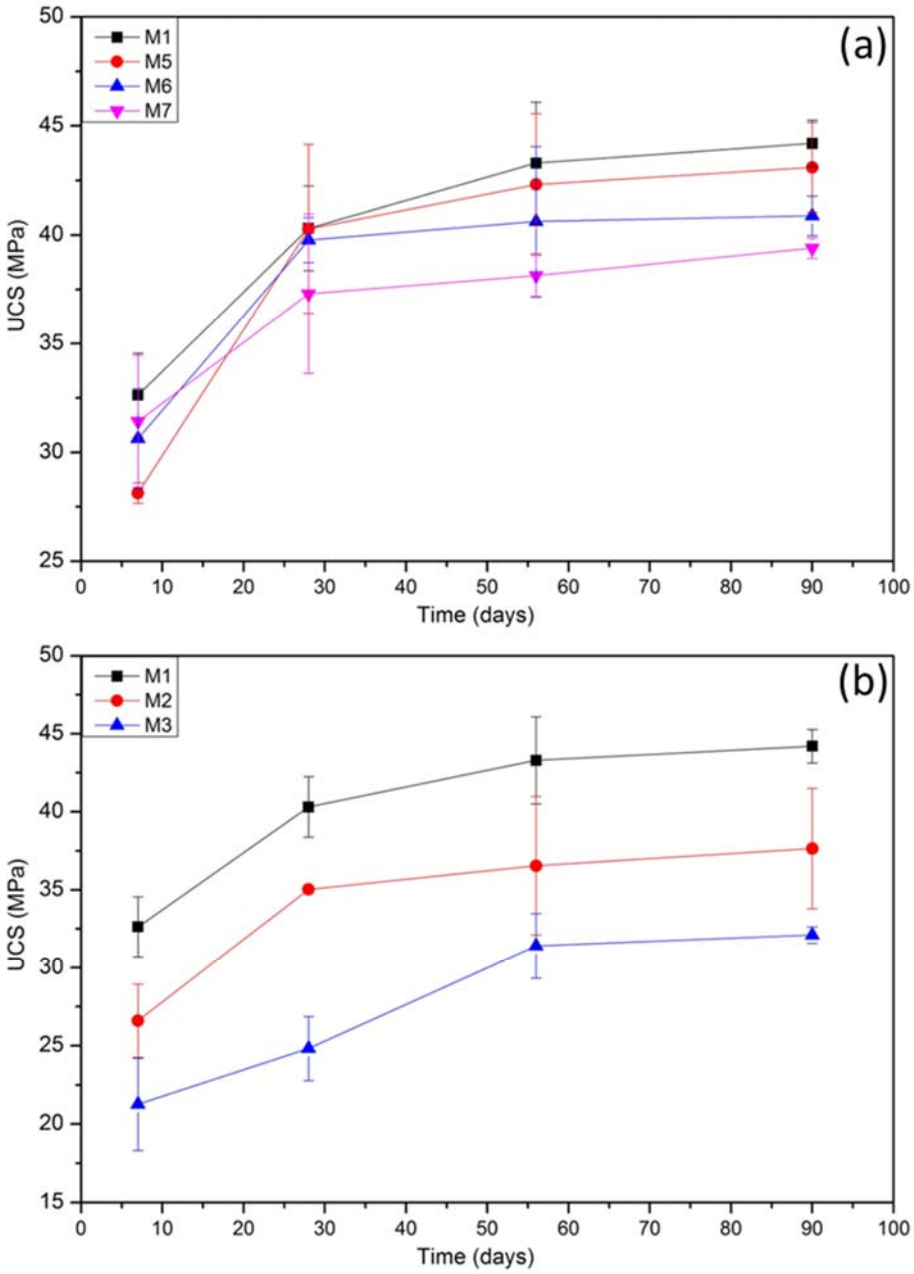

Figure 15: UCS of mortar samples containing different sizes of: (a) CP_M1, and (b) PP_MB at different ages.

5 Conclusions

In this paper, the development of pellets and encapsulation in a PVA-based coating for potential healing agents was investigated as a system to improve self-healing properties of cement-based composites. Two commercial types of MgO-based pellets in addition to two developed prototype pellets were examined; their characteristics and the PVA coating were evaluated. The influence of the coated pellets on the workability and hydration process of the fresh mortar mixtures and

on the compressive strength of hardened mortar specimens was examined; the pellets replaced sand in mortar mixes by different proportions.

The developed prototype pellets exhibited several similar physical and mechanical properties compared to the two commercial types of MgO pellets. In comparison with the sand used, both of the prototype and commercial pellets used here demonstrated approximately 20% higher porosity and not more than one-third of the crushing strength. This would be considered as an advantage as the pellets are needed to rupture and disintegrate upon cracking into the cementitious matrix.

Encapsulation of the active minerals into a PVA coating resulted in promising results as the coating material maintained integrity and stability in water and high pH solutions. This was associated with a decrease in mechanical properties in both environments, which needs to be explored. When applied on pellets, PVA coating was required to be sprayed in three layers to cover the entire surface of pellet. The thickness of coating ranged between 10µm and 50µm. Moreover, the coated pellets showed an increase in their crushing strength by ~ 15-105%. In mortar mixtures, the characterisation of fresh mortars by using flowability and calorimetry tests showed negligible effect when SHP replaced up to10% of sand weight. This replacement caused a reduction in compressive strength of mortar samples by less than 15% in all cases. Overall, this study has introduced the basic design and characterisation concepts of developing pellets for self-healing cement-based composites. A further study, which is to verify the healing efficiency of the coated pellets, will be conducted.

6 Acknowledgments

The financial support of the PhD scholarship for the first author from the Yousef Jameel Foundation through Cambridge Commonwealth, European & International Trust is gratefully acknowledged. Support from the Engineering and Physical Sciences Research Council (EPSRC - UK) for the Materials for Life project (Project Ref. EP/K026631/1) is also gratefully acknowledged.

7 References

[1] H. Huang, G. Ye, C. Qian, and E. Schlangen, Self-healing in cementitious materials: Materials, methods and service conditions, *Mater. Des.*, vol. 92, pp. 499–511, 2016.

[2] D. Rooij, M. R., and E. Schlangen, Self-healing phenomena in cement-based materials-State-of-the-Art report of RILEM Technical Committee, 2011.

[3] M. Wu, B. Johannesson, and M. Geiker, A review: Self-healing in cementitious materials and engineered cementitious composite as a self-healing material, *Constr. Build. Mater.*, vol. 28, no. 1, pp. 571–583, Mar. 2012.

[4] C. Edvardsen, Water permeability and autogenous healing of cracks in concrete, *ACI Mater. J.*, vol. 96, no. 4, pp. 448–454, 1999.

[5] H.-W. Reinhardt and M. Jooss, Permeability and self-healing of cracked concrete as a function of temperature and crack width, *Cem. Concr. Res.*, vol. 33, no. 7, pp. 981–985, Jul. 2003.

[6] V. C. Li and E.-H. Yang, Self healing in concrete materials, in *Self healing materials*, Springer, 2007, pp. 161–193.

[7] E. Cuenca and L. Ferrara, Self-healing capacity of fiber reinforced cementitious composites. State of the art and perspectives, *KSCE J. Civ. Eng.*, vol. 21, no. 7, pp. 2777–2789, 2017.

[8] R. P. Borg, E. Cuenca, E. M. Gastaldo Brac, and L. Ferrara, Crack sealing capacity in chloride-rich environments of mortars containing different cement substitutes and crystalline admixtures, *J. Sustain. Cem. Mater.*, vol. 7, no. 3, pp. 141–159, 2018.

[9] L. Ferrara *et al.*, Experimental characterization of the self-healing capacity of cement based materials and its effects on the material performance: A state of the art report by COST Action SARCOS WG2, *Constr. Build. Mater.*, vol. 167, pp. 115–142, 2018.

[10] T. Qureshi and A. Al-Tabbaa, Self-healing of drying shrinkage cracks in cement-based materials incorporating reactive MgO, *Smart Mater. Struct.*, vol. 25, no. 8, pp. 1–16, 2016.

[11] S. Nagataki and H. Gomi, Expansive admixtures (mainly ettringite), *Cem. Concr. Compos.*, vol. 20, pp. 163–170, 1998.

[12] R. Sahamitmongkol and T. Kishi, Tensile behavior of restrained expansive mortar and concrete, *Cem. Concr. Compos.*, vol. 33, no. 1, pp. 131–141, 2011.

[13] Y.-S. Lee and J.-S. Ryou, Self healing behavior for crack closing of expansive agent via granulation/film coating method, *Constr. Build. Mater.*, vol. 71, pp. 188–193, 2014.

[14] S. A. L. de Koster, R. M. Mors, H. W. Nugteren, H. M. Jonkers, G. M. H. Meesters, and J. R. van Ommen, Geopolymer Coating of Bacteria-containing Granules for Use in Self-healing Concrete, *Procedia Eng.*, vol. 102, pp. 475–484, 2015.

[15] L. Lv *et al.*, Synthesis and characterization of a new polymeric microcapsule and feasibility investigation in self-healing cementitious materials, *Constr. Build. Mater.*, vol. 105, pp. 487–495, 2016.

[16] K. Van Tittelboom and N. De Belie, Self-healing in cementitious materials - a review, *Materials (Basel).*, vol. 6, no. 6, pp. 2182–2217, May 2013.

[17] C. Du, A Review of Magnesium Oxide in Concrete, *Concr. Int.*, vol. 27, no. 12, pp. 45–

50, 2005.

[18] E. Gartner, Industrially interesting approaches to "low-CO_2" cements, *Cem. Concr. Res.*, vol. 34, no. 9, pp. 1489–1498, 2004.

[19] A. R. Sakulich, Reinforced geopolymer composites for enhanced material greenness and durability, *Sustain. Cities Soc.*, vol. 1, no. 4, pp. 195–210, 2011.

[20] A. Bras, R. Gião, V. Lúcio, and C. Chastre, Development of an injectable grout for concrete repair and strengthening, *Cem. Concr. Compos.*, vol. 37, no. 1, pp. 185–195, 2013.

[21] A. Farahani, H. Taghaddos, and M. Shekarchi, Prediction of long-term chloride diffusion in silica fume concrete in a marine environment, *Cem. Concr. Compos.*, vol. 59, pp. 10–17, 2015.

[22] W. H. Engelleitner, Binders: how they work and how to select one, *Powder bulk Eng.*, vol. 15, no. 2, pp. 31–37, 2001.

[23] S. P. E. Forsmo, a. J. Apelqvist, B. M. T. Björkman, and P.-O. Samskog, Binding mechanisms in wet iron ore green pellets with a bentonite binder, *Powder Technol.*, vol. 169, no. 3, pp. 147–158, Nov. 2006.

[24] T. H. Ahn and T. Kishi, The effect of geo-materials on the autogenous healing behavior of cracked concrete, in *Proceedings of 2nd International Conference on Concrete Repair, Rehabilitation and Retrofitting*, 2008, no. 1, pp. 24–26.

[25] J. S. Park, J. W. Park, and E. Ruckenstein, Thermal and dynamic mechanical analysis of PVA/MC blend hydrogels, *Polymer (Guildf).*, vol. 42, no. 9, pp. 4271–4280, 2001.

[26] C. A. Finch, *Polyvinyl alcohol: developments*. Wiley, 1992.

[27] L. W. Chan, J. S. Hao, and P. W. S. Heng, Evaluation of Permeability and Mechanical Properties of Composite Polyvinyl Alcohol Films., *Chem. Pharm. Bull. (Tokyo).*, vol. 47, no. 10, pp. 1412–1416, 1999.

[28] F. Jin, Characterisation and Performance of Reactive MgO-based Cements with Supplementary Cementitious Materials, University of Cambridge, 2014.

[29] S. H. Imam, P. Cinelli, S. H. Gordon, and E. Chiellini, Characterization of biodegradable composite films prepared from blends of poly(vinyl alcohol), cornstarch, and lignocellulosic fiber, *J. Polym. Environ.*, vol. 13, no. 1, pp. 47–55, 2005.

[30] X. Han, S. Chen, and X. Hu, Controlled-release fertilizer encapsulated by starch/polyvinyl alcohol coating, *Desalination*, vol. 240, no. 1, pp. 21–26, 2009.

[31] J. P. Pérez and M. Rabišková, Influence of the drying technique on theophylline pellets prepared by extrusion-spheronization, *Int. J. Pharm.*, vol. 242, no. 1–2, pp. 349–351, 2002.

[32] R. Ramachandran *et al.*, Experimental studies on distributions of granule size, binder content and porosity in batch drum granulation: Inferences on process modelling requirements and process sensitivities, *Powder Technol.*, vol. 188, no. 2, pp. 89–101, 2008.

[33] E. P. Cox, A Method of Assigning Numerical and Percentage Values to the Degree of Roundness of Sand Grains, *J. Paleontol.*, vol. 1, no. 3, pp. 179–183, 1927.

[34] W. J. Priest, Swelling of polyvinyl alcohol in water, *J. Polym. Sci.*, vol. 6, no. 6, pp. 699–710, 1951.

[35] R. W. Korsmeyer, R. Gurny, E. Doelker, P. Buri, and N. A. Peppas, Mechanisms of solute release from porous hydrophilic polymers, *Int. J. Pharm.*, vol. 15, no. 1, pp. 25–35, 1983.

[36] T. F. Tadros, Adsorption of polyvinyl alcohol on silica at various ph values and its effect on the flocculation of the dispersion, *J. Colloid Interface Sci.*, vol. 64, no. 1, pp. 36–47, 1978.

[37] O. M. Y. Koo *et al.*, Investigation into stability of poly(vinyl alcohol)-based Opadry films., *AAPS PharmSciTech*, vol. 12, no. 2, pp. 746–754, 2011.

[38] R. F. Landel and L. E. Nielsen, *Mechanical properties of polymers and composites*. CRC Press, 1993.

[39] F. Podczeck and S. M. Almeida, Determination of the mechanical properties of pellets and film coated pellets using Dynamic Mechanical Analysis (DMA), *Eur. J. Pharm. Sci.*, vol. 16, no. 3, pp. 209–214, 2002.

[40] R. D. Holtz and W. D. Kovacs, *An introduction to geotechnical engineering*. 1981.

[41] H. F. W. Taylor, *Cement chemistry*. Thomas Telford, 1997.

[42] M. Sonebi, Report on Measurements of Workability and Rheology of Fresh Concrete, 2010.

[43] T. Nochaiya, W. Wongkeo, and A. Chaipanich, Utilization of fly ash with silica fume and properties of Portland cement-fly ash-silica fume concrete, *Fuel*, vol. 89, no. 3, pp. 768–774, 2010.

[44] D. King, The effect of silica fume on the properties of concrete as defined in concrete society report 74, cementitious materials, *Our world Concr. Struct.*, pp. 1–23, 2012.

[45] V. V. Hung and T. Kishi, Water-tightness performance of crack-self healing concrete incorporating various types of granule of supplementary cementitious materials and/or Portland cement and other additives, in *In The Second International Conference on Sustainable Construction Materials and Technologies*, 2013, pp. 138–147.

[46] P. Sun and H. C. Wu, Transition from brittle to ductile behavior of fly ash using PVA fibers, *Cem. Concr. Compos.*, vol. 30, no. 1, pp. 29–36, 2008.

[47] B. Felekoğlu, K. Tosun, and B. Baradan, Effects of fibre type and matrix structure on the mechanical performance of self-compacting micro-concrete composites, *Cem. Concr. Res.*, vol. 39, no. 11, pp. 1023–1032, 2009.

[48] T. Kanda and V. C. Li, Interface Property and Apparent Strength of High-Strength Hydrophilic Fiber in Cement Matrix, *J. Mater. Civ. Eng.*, vol. 10, no. 1, pp. 5–13, 1998.

[49] N. Banthia, V. Bindiganavile, J. Jones, and J. Novak, Fiber-reinforced concrete in precast concrete applications: Research leads to innovative products, *PCI J.*, vol. 57, no. 3, pp. 33–46, 2012.

[50] M. M. Pelletier, R. Brown, A. Shukla, and A. Bose, Self-healing concrete with a microencapsulated healing agent, *Univ. Rhode Island, Kingston,USA*, no. C, 2011.